Observation of the Ground Subsidence in the Abandoned Gaeun Coal Mining Area using JERS-1 SAR

Hahn Chul Jung, Sang-Wan Kim, Kyung Duck Min, and Joong-Sun Won
Dept. of Earth System Sciences, Yonsei University
134 Shinchon-dong Seodaemun-gu, Seoul, Korea 120-749
hcjung75@hotmail.com

Abstract: The ground subsidence that occurred in an abandoned coal mining area, Gaeun, Korea, was observed by using 25 JERS-1 SAR interferograms from November 1992 to October 1998. We estimated the subsidence on a subset of image pixels corresponding to point-wise permanent scatters (PSs) by exploiting a long temporal series of interferometric phases. The results were compared it with a distribution map of *in situ* examined crack level. PSs were identified by means of amplitude dispersion index and coherence of the interferograms. The measured subsidence rate represented the average velocity in a period of image acquisition and excluded complex nonlinear displacements such as an abrupt collapse. The mean line-of-sight velocity in the study area is 0.19cm/yr and an r.m.s. error is 0.18cm/yr. The center of the abandoned Gaeun coal mine (0.49cm/yr) and the area near to the Gaeun station (1.66cm/yr) were observed as most rapidly subsiding areas.

Key words: Coal mine, subsidence, JERS-1, PSInSAR, Gaeun

1. Introduction

Causes for ground subsidence at rates higher than a few mm/year include ground water pumping, hydrocarbon extraction, active or abandoned mining, etc. There are increasing demands for monitoring surface deformation. SAR interferometry is one possible technique for surface deformation mapping or one possible element of an integrated monitoring strategy. However, temporal and geometrical decorrelations often prevent SAR interferometry from being an operational tool for surface deformation monitoring and topographic profile reconstruction [7]. The relative unsatisfying visible spatial resolution with respect to the ground distortion is caused by residual phase noise of the differential interferograms. These drawbacks can be overcome by carrying out measurements on a subset of image pixels corresponding to point-wise stable reflector (or permanent scatterer: PS) and exploiting a long temporal series of interferometric phases [4]. On these pixels, submeter DEM accuracy and millimetric terrain motion detection can be achieved.

In this paper, we will discuss the application results of permanent scattering interferometry over an abandoned coal mining area. The study site is a region approximately 2×1 km wide in the Gaeun region, Korea. The area is of high geophysical interest because it is known to be unstable due to abandoned coal mines [2], [3]. Fig. 1 shows aerial photograph of the study area.

2. Data and Method

1) Interferogram Formation

Since the area was strongly affected by temporal decorrelation, the analysis was carried out in a multi-image framework. We analyzed a series of JERS-1 (L-band, 1.3GHz, 23.5cm in wavelength) SAR images between 1992 and 1998 to observe ground surface deformation. Data sets as many as possible lead to an improved temporal resolution of non-linear deformation. The 2-pass was used to derive the differential interferograms indicated in Table 1. It summarizes coherence mean, elapsed time, and perpendicular baseline of the interferometric pairs used. The initial baseline estimates based on orbit data were improved by rectifying the orbit with a simulated SAR image from DEM.

2) The PS Technique

The permanent scatterer radar interferometry (PSInSAR) is a further development from the DInSAR method and was invented by POLIMI group of Italy. The approach is a processing technique aimed at isolating the different phase terms (atmospheric phase screen

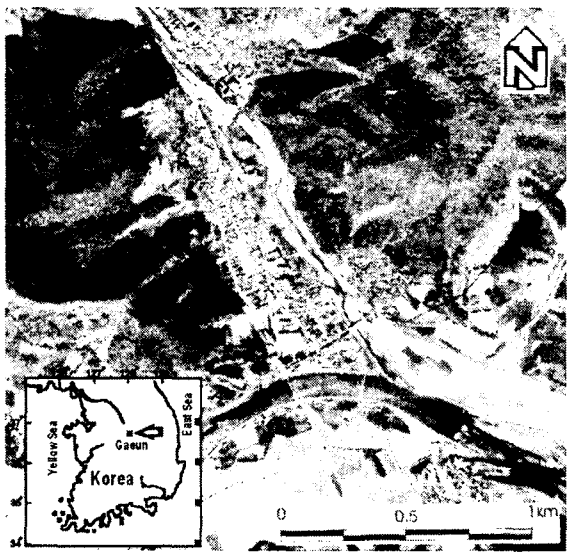

Fig. 1. Location map and an aerial photograph of the study area.

Table 1. Summary of the JERS-1 SAR interferometric pairs.

No.	SAR image		Perpendicular baseline (Ambiguity height) [m]	Time interval [days]	Coherence mean
	Master	Slave			
1	96/10/27	92/11/05	982.3(-51.0)	-1452	0.27
2		92/12/19	462.2(-108.4)	-1408	0.30
3		93/03/17	554.5(-90.4)	-1320	0.29
4		93/06/13	-635.8(78.8)	-1232	0.28
5		93/07/27	1002.5(-50.0)	-1188	0.27
6		93/09/09	1285.6(-39.0)	-1144	0.27
7		93/10/23	1034.8(-48.4)	-1100	0.29
8		93/12/06	2117.1(-23.7)	-1056	0.24
9		94/01/19	1464.7(-34.2)	-1012	0.27
10		95/02/19	-2399.9(20.9)	-616	0.24
11		96/03/21	-1309.4(38.3)	-220	0.30
12		96/07/31	270.1(-185.5)	-88	0.39
13		96/12/10	1271.0(-39.4)	44	0.33
14		97/01/23	800.6(-62.6)	88	0.33
15		97/03/08	546.3(-91.7)	132	0.38
16		97/06/04	488.9(-102.5)	220	0.35
17		97/10/14	-3366.1(14.9)	352	0.21
18		97/11/27	-2210.7(22.7)	396	0.25
19		98/01/10	-1912.0(26.2)	440	0.26
20		98/02/23	-2389.2(21.0)	484	0.25
21		98/04/08	-3181.7(15.7)	528	0.21
22		98/05/22	571.9(-87.6)	572	0.31
23		98/07/05	-3042.4(16.5)	616	0.21
24		98/08/18	-1895.3(26.4)	660	0.26
25		98/10/01	-1557.8(32.2)	704	0.28

deformation, and residual topography) on a sparse grid of phase stable, point-wise radar targets. The main steps of the technique can be summarized as follows: 1) Interferogram formation, 2) Digital Elevation Model and differential interferograms formation, 3) Preliminary estimate of LOS motion, elevation error, and atmospheric contribution, and 4) Refinement of step 3. Detailed description of the processing technique can be found in [5], [6], and [7]. PSs are only slightly affected by decorrelation and can be used to estimate and remove the atmospheric phase screen.

3. Results

1) PS Candidates Selection

In order to select PS candidates, we calculated a time series of the amplitude values of each pixel in the area of interest as well as coherence map. If a target exhibits a coherence always greater than a certain value, that is selected as a PS candidate (PSC). However, due to the high dispersion of the baseline values and the limited accuracy of the DEM, some coherence maps turn out to be useless. Coherence computation implies space averaging of the data inside a sub-window [7]. Thus, we used a pixel-by-pixel analysis of the amplitude returns relative to each SAR image to choose stable point targets and excluded interferograms having larger than 1,500 m perpendicular baseline.

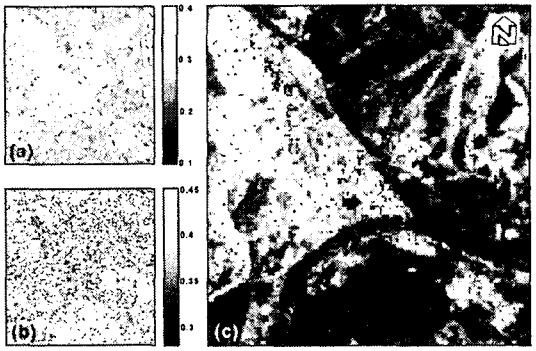

Fig. 2. PSC Selection. (a) Coherence map, (b) amplitude dispersion index, and (c) PSC. Blue dots satisfy the condition (coherence > 0.3); red dots satisfy the condition (amplitude dispersion index < 0.3); and green dots (PSC) satisfy both conditions.

PSCs were selected when amplitude dispersion index was lower than 0.3 and all coherence values of the 15 interferograms were higher than 0.3. Fig. 2(a) and (b) represent coherence map and amplitude dispersion index map of the study site. Fig. 2(c) represents PSCs satisfying both conditions.

2) PS Identification

After PSC selection, elevation errors and LOS velocities of the PSC were computed by means of an iterative algorithm and then atmospheric components were estimated on the uniform image grid. After removal of atmospheric phase contribution, one could compute elevation errors and target velocity on a pixel-by-pixel basis [7]. Therefore we can analyze most phenomena that contribute to the phase values such as terrain deformation, DEM errors, orbit indetermination, and atmospheric disturbance.

Fig. 3(a) represents the phase contributions for a LOS velocity of –0.4cm/yr. and a height error of -15 m, which were estimated from the 25 wrapped interferograms available with a joint estimation. Fig. 3(b) represents an example of the differential phase values plotted versus normal baseline of each acquisition for a PS, and an example of a time series of the differential phase values for the estimation of the selected point. Each slope of the fitted straight line is the local height error and LOS velocity, respectively. Although the results obtained with this technique were useful, the algorithm does not account for nonlinear target motion: coherent scatterers undergoing a complex motion are not identified as PSs, or, in other cases, the nonlinear term of their motion is considered as part of the atmospheric contribution [6].

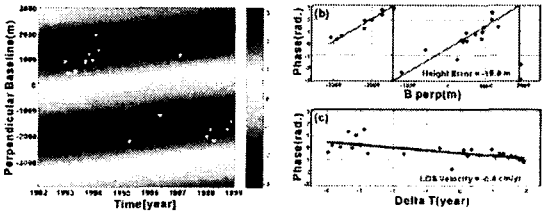

Fig. 3. (a) Space-time distribution of the available data. The bi-dimensional complex sinusoid represents the phase contribution for a LOS velocity of -0.4 cm/yr and a height error of -15 m. (b)-(c) Regression of interferometric phase differences between pair of point targets with respect to baseline and time.

3) Subsidence Rate

Fig. 4 represents the estimated LOS velocity field and location of the PSs. More than 100 permanent scatterers were identified in the area of investigation. As for PS density, the total number of stable scatterers in the study site is relatively small because the area is mountainous region subject to temporal decorrelation. Most of the identified PSs were observed in the urbanized area. Coal Industry Promotion Board, Korea, assessed its ground stability in 1997 based on crack classification and standard suggested by [1]. G1, G2, and G3 were influenced by the Gaeun coal mine abandoned in 1976 and their buildings were damaged or cracked; on an average, G1 was over 15 mm, G2 was 5~15 mm, and G3 was under 5 mm in crack width [2], [3]. The mean LOS velocities of the PSs identified in G1, G2, and G3 were 0.49, 0.30, and 0.19 cm/yr, respectively. The order of group's subsidence rates calculated through PS technique fits well that of group's crack level. The most highly subsiding area was near to Gaeun train station and the mean LOS velocity of its detected 5 PSs was 1.66 cm/yr. The area except G1, G2, G3, and G4 was not affected by an abandoned coal mine and considered to be stable. Table 2 summarizes the number of PSs, LOS velocity, and crack level of five groups. Fig. 5 represents the temporal series evolution of four PSs. Each PS was selected once in G1, G2, G3, and G4. The higher LOS velocity

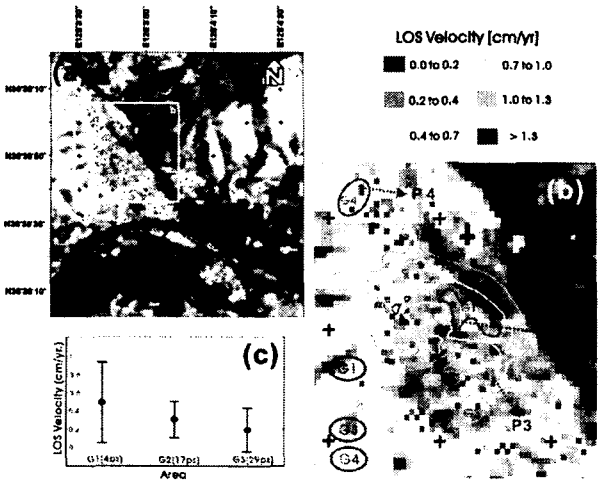

Fig. 4. Estimated LOS velocity and location of PSs.

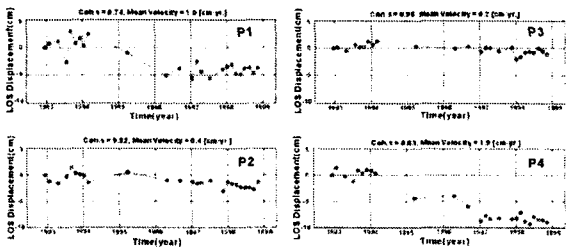

Fig. 5. Temporal series evolution (from 1992 to 1998) of the displacement of four selected permanent scatterers.

value is, the steeper the slope of the fitted straight line. The higher coherence value, the better linear velocity model fits the subsidence pattern of PS. Consequently, G1, G2, and G4 are expected to subside and the residue areas are considered to be stable.

4. Conclusions

We estimated the subsidences occurred in the

Table 2. Estimated subsidence rates of five groups located in the center of the Wangreunglee area.

Group	No. of detected PS	Subsidence rate [cm/yr, LOS]		Crack level [width, mm]	Remarks
		Mean	Std. Dev.		
G1	4	0.49	0.44	Severe (>15)	
G2	17	0.30	0.20	Moderate (5~15)	- Areas influenced by the Gaeun coal mine abandoned in 1976.
G3	29	0.19	0.24	Slight (<5)	
G4	5	1.66	0.55	No field data	- the area across from Gacun station and expected to be the most highly subsiding.
G_R	80	0.19	0.21	No field data	- the area except G1, G2, G3, and G4.

Gaeun area, Korea, from November 1992 to October 1998 by using 26 JERS-1 SAR interferograms. The center of the abandoned Gaeun coal mine (0.49cm/yr) and the area near to Gaeun station (1.66cm/yr) were observed as the most significantly subsiding areas. The estimated subsidence rate represents the average velocity in a period of image acquisition but excluds complex nonlinear displacements such as an abrupt collapse. The major advantages of the PS approach are the suitability for wide area monitoring coupled with the capability to provide deformation data relative to single targets. However, the performances are limited by the intrinsic ambiguity of phase measurements (enabling the detection of slow deformation only) and by the capability of providing one dimensional displacement data. Further study comparing with ground measurement data will follow. This study demonstrates a potential of L-band PSInSAR to measure ground subsidence where there is of high temporal decorrelation for vegetated areas.

References

[1] Bruhn, W. R., Speck, R. C. and Thill, R. E. (1983) The Appalachian Field: Damage to structures above active underground mines, Surface Mining Environmental Monitoring and Reclamation Handbook, Elsevier, New York, p. 656-669.

[2] Coal industry promotion board (1997) Geological and principal research for the ground stability assessment on the mined-out area in Munkyong Region.

[3] Coal industry promotion board (2000) Investigation into ground stability in Munkyong Region.

[4] Colesanti, C., Ferrett,i A., Ferrucci, F., Prati, C., and Rocca, F. (2003) Monitoring landslides and tectonic motions with the Permanent Scatterers Technique, Engineering Geology, v. 68, p. 3-14.

[5] Ferretti, A., Prati, C., and Rocca, F. (1999) Non-Uniform Motion Monitoring Using the Permanent Scatterers Technique, Fringes '99.

[6] Ferretti, A., Prati, C., and Rocca, F. (2000) Nonlinear Subsidence Rate Estimation Using Permanent Scatterers in Differential SAR Interferometry, IEEE Transaction on Geoscience and Remote Sensing, v. 38, p. 2202-2212.

[7] Ferretti, A., Prati, C., and Rocca, F. (2001) Permanent Scatterers in SAR Interferometry, IEEE Transaction on Geoscience and Remote Sensing, v. 39, p. 8-20.

[8] Kim, S.W., Lee, C.W., and Won, J.S. (2002) Ground Subsidence Estimation in a Coastal Reclaimed Land Using JERS-1 L-band SAR Interferometry, Korea Society of Econ. Environ. Geol, 35(5), pp. 465-478.

[9] Marple, S. L. (1987) Digital Spectral Analysis with Applications, Englewood Cliffs, Prentice-Hall.

[10] Massonnet, D., Briole, P., and Arnaud A. (1993) Deflation of Mount Etna monitored by spaceborne radar interferometry. Nature, v. 375, p. 441-500.

[11] Zebker, H. A., Rosen P. A., Goldstein, R. M., Gabriel, A., and Werner, C. L. (1994) On the derivation of coseismic displacement fields using differential radar interferometry: The Landers earthquake, Journal of Geophysical Research, v. 99, p. 19617-19634.